

Video Article

Diffusion Imaging in the Rat Cervical Spinal Cord

Elizabeth Zakszewski¹, Brian Schmit², Shekar Kurpad¹, Matthew D. Budde¹¹Department of Neurosurgery, Medical College of Wisconsin²Department of Biomedical Engineering, Marquette UniversityCorrespondence to: Elizabeth Zakszewski at ezakszewski@mcw.eduURL: <https://www.jove.com/video/52390>DOI: [doi:10.3791/52390](https://doi.org/10.3791/52390)

Keywords: Neurobiology, Issue 98, spinal cord, magnetic resonance imaging, diffusion tensor imaging, respiratory gating, diffusion kurtosis imaging, rat, spine

Date Published: 4/7/2015

Citation: Zakszewski, E., Schmit, B., Kurpad, S., Budde, M.D. Diffusion Imaging in the Rat Cervical Spinal Cord. *J. Vis. Exp.* (98), e52390, doi:10.3791/52390 (2015).

Abstract

Magnetic resonance imaging (MRI) is the state of the art approach for assessing the status of the spinal cord noninvasively, and can be used as a diagnostic and prognostic tool in cases of disease or injury. Diffusion weighted imaging (DWI), is sensitive to the thermal motion of water molecules and allows for inferences of tissue microstructure. This report describes a protocol to acquire and analyze DWI of the rat cervical spinal cord on a small-bore animal system. It demonstrates an imaging setup for the live anesthetized animal and recommends a DWI acquisition protocol for high-quality imaging, which includes stabilization of the cord and control of respiratory motion. Measurements with diffusion weighting along different directions and magnitudes (b-values) are used. Finally, several mathematical models of the resulting signal are used to derive maps of the diffusion processes within the spinal cord tissue that provide insight into the normal cord and can be used to monitor injury or disease processes noninvasively.

Video Link

The video component of this article can be found at <https://www.jove.com/video/52390/>

Introduction

Magnetic resonance imaging (MRI) is a noninvasive tool that provides a window into the brain and spinal cord in both health and disease. MRI has revolutionized clinical diagnosis, but it is also a valuable tool for laboratory investigation. Animal models of neurological injury or disease provide a platform to understand the pathophysiology and accelerate discovery of therapies. In this report, we demonstrate the application of MRI to a rat model of spinal cord injury to investigate potential biomarkers of microstructural injury¹ using diffusion tensor imaging (DTI). The potential discovery of imaging biomarkers will help in the diagnosis and management of patients with spinal cord injury. These markers are likely to play a role in discovery of therapies in preclinical models and enable observation or prognosis in their translation to the clinical setting.

DTI is a specialized form of MRI that measures microscopic motion of water molecules (*i.e.* diffusion). DTI has been particularly advantageous in the nervous system due to the presence of axons where diffusion is disproportionately faster along the axons than perpendicular to them, which provides information regarding their orientation and microstructural composition. Scalar indices derived from DTI, including a measure of the overall diffusion within the tissue, mean diffusivity (MD), and a measure of the orientation dependence of diffusion, fractional anisotropy (FA)^{2,3}, have seen extensive applications in characterizing the microstructure of the nervous system in both health and disease⁴. These metrics have revealed microscopic tissue features that are invisible through most other MRI methods. Previous efforts demonstrated that DTI detects remote microstructural changes within the cervical cord following thoracic SCI in rats¹. The DTI changes remote from the lesion likely reflect how the entire spinal cord responds to injury, and are potentially a marker of secondary injury.

Imaging the rat spinal cord *in vivo* presents several unique challenges. Most notably, the spinal cord is affected by respiratory motion and requires careful attention to minimize motion using several methods. In past studies, immobilization devices removed motion of the spinal column during scanning⁵. For imaging of the cervical cord, we utilize physical restraint in the form of a head holder and ear bars, which attenuates, but does not eliminate motion caused by respiration. Furthermore, we utilize a custom respiratory gating scheme to synchronize image acquisition with the respiratory cycle in an efficient manner. These modifications enable removal of the artifacts otherwise caused by the large-scale bulk motion caused by respiration⁶. DWI is highly sensitive to microscopic motion, including CSF flow and blood pulsation, and these smaller sources of motion contamination are also alleviated by the respiratory gating scheme. Additionally, the spinal cord has a small cross sectional area and represents only a fraction of the field of view. For cervical spine imaging, in which the spinal cord is situated deep within the body of the animal, a cylindrical radiofrequency coil with adequate signal penetration is needed to image the cervical spinal cord with high resolution. A reduction in the field of view is achieved by outer volume suppression (OVS), which also serves to cancel, or spoil, the signal from tissues outside of the spinal cord. This method, called spoiler gradients or outer volume suppression, also serves to reduce any contamination of residual animal motion, CSF flow, or blood pulsation within these tissues.

The arrangement of the spinal cord can also be exploited to simplify the imaging protocol. The spinal cord axons in the white matter (WM) are nearly all oriented parallel to the main axis of the spinal cord. Thus, whereas DWI of the brain requires measurements along at least 6

directions to ensure the results do not depend on the position within the magnet (a process called diffusion tensor imaging), measurements in the spinal cord can be acquired only along 2 directions parallel and perpendicular to the cord^{7,8}, hereafter referred to as longitudinal and transverse, respectively. Thus, the diffusivity and other parameters are measured along the 2 directions separately and allow inferences into the microstructure of the tissue in both health and disease or injury.

Protocol

NOTE: Ethics Statement: The Institutional Care and Use Committees (IACUC) of the Medical College of Wisconsin and the Clement J. Zablocki VA Medical Center approved all procedures.

1. Animal Preparation and Monitoring

1. Anesthetize the rat in an induction chamber, using 5% isoflurane in medical air. When the righting reflex is absent and squeezing the hind paw produces no withdrawal reflex, reduce anesthesia to 2% and transfer the animal to the scanner bed in a head-first prone position. Maintain 2% isoflurane through a nose cone device throughout the procedure, and keep medical air at a flow rate of approximately 1 L/min. Apply a small amount of lubricating ointment to the rat's eyes to avoid damage to the cornea while under anesthesia.
2. Place a respiratory monitoring belt securely around the rat's torso. Connect the belt to a respiratory gating system. Before advancing the rat into the scanner bore, check the respiratory monitoring computer to ensure the respiratory cycle is clear and consistent. Adjust the belt if necessary, since this step is imperative for image quality.
3. Monitor and maintain the animal's body temperature at 37 °C through a rectal probe and warm air heating system. Maintain the respiratory rate between 30-45 breaths per min by adjusting the level of anesthesia between 1.2 and 2%.
4. Position the rat in the head holder with a bite bar and screw-in ear bars (**Figure 1**), and slide the head into a quadrature volume coil until the cervical spine is positioned in the center of the coil.
NOTE: The rat's shoulders may prevent further progression into the coil.
5. Advance the rat and supporting holders into the scanner bore. If applicable, adjust the tuning and matching capacitors of the coil to the proper frequency and impedance according to the instructions provided by the coil vendor.

2. MRI Scanning Parameters

NOTE: The procedures described here used a 9.4 T horizontal bore small animal system but are applicable to other field strengths of small animal MRI systems.

1. Use the MRI system's automated procedures for detection of the resonance frequency, iteratively improving the homogeneity of the magnetic field (shimming), calibration of the radiofrequency power, and adjustment of the receiver gain.
2. Using the system's software interface, obtain a default three-plane scout scan to ensure correct positioning.
 1. Click "New scan", select tripilot, and click the "traffic light" to acquire the images.
 2. Ensure the center of the cervical spine is aligned with both the center of the magnet and the center of the MRI coil. To center the spine within the magnet, push or pull on the cradle and reacquire the scout scan for verification.
 3. To adjust the position of the cervical spine relative to the MRI coil, remove the cradle from the magnet for repositioning. If necessary, repeat this process until the position is consistent. If the animal is repositioned, repeat step 2.1.
3. Add a new echo-planar diffusion weighted spin-echo sequence (DtEpi) to the current imaging protocol.
 1. Configure and acquire diffusion weighted images with the DWI sequence using the default settings except for the following:
 2. Open the slice position graphical interface to prescribe 12 slices with a thickness of 0.75 mm. Orient the slices perpendicular to the main axis of the cervical cord. Ensure consistent slice positioning between different animals or across different imaging sessions using the base of the cerebellum as an internal reference.
 3. Set the saturation bands to 'on'. Position 4 saturation bands with a thickness of 10 mm outside of the spinal cord to minimize the signal from these tissues and reduce their potential to induce artifacts (**Figure 3**). Set respiratory gating ('trigger module') to 'on'.
NOTE: The custom respiratory gating requires knowledge and experience in pulse sequence programming. If this is not available, a workaround is to reduce the number of slices to 3-5 and the TR to 1 s to ensure that all slices are obtained in-between breaths of the animal. Repeat the full sequence with the other subset of slices to obtain the full coverage of the cervical cord.
 4. Click the toolbox icon and then click "Edit method." Set the number of EPI segments to 4. Change the phase encoding direction to left-right. Other default settings should be: echo spacing = 0.3234 ms, total echo train length per EPI segment = 32.
NOTE: The phase encoding set to the left-right direction rather than anterior-posterior will reduce the contamination of motion from other structures.
 5. Use the following geometrical settings. Matrix size = 128 x 128, and in-plane field-of-view = 25.6 x 25.6 mm, resulting in an in-plane spatial resolution = 0.200 x 0.200 mm. Ensure slice thickness = 0.75 mm. Slice order = 'interleaved', slice gap = 0 mm.
 6. Use the following diffusion weighting settings: DW measure mode = 'DW contrast', diffusion gradient duration (δ) = 7 ms, diffusion gradient separation (Δ) = 12 ms, number of b-values = 8, desired b-values = 0, 250, 500, 750, 1,000, 1,500, 2,500, 3,500 mm²/s², number of diffusion directions = 2, diffusion weighting directions = [1 0 0] and [0 0 1] (made to be in the planes parallel and orthogonal to the spinal cord axis).
NOTE: With these settings, we achieved b-values as high as 3,500 s/mm². Hardware specifications and other system performance characteristics may limit the b-value, since diffusion gradient duration (δ) and diffusion gradient separation (Δ) are dependent on the gradient performance, which on our system were: (maximum gradient strength: 440 mT/m, maximum slew rate: 3,440 T/m/s). For measurements of kurtosis, 2 b-values, with the higher b-value of at least 2,000 s/mm², are recommended.
 7. Use the following timing settings. echo time (TE) = 27 ms (set to minimum by entering 0), repetition time (TR) = 1,800 msec.
4. Acquire the prepared sequence. With the parameters listed above, the total acquisition time is approximately 25 min.

5. Throughout all scans, monitor the respiratory gating software and adjust the delay period between the “trigger” (software detection of expiration) and the signal to the MRI system so that acquisitions occur only in the quiescent (unmoving) portion of the respiratory cycle (**Figure 2a**, stable portion of gray line). A trigger delay between 100–400 msec is necessary depending on the animal’s respiration pattern. This will help to reduce artifacts that occur with respiratory motion (**Figure 3e**).
6. If available, repeat the sequence with the custom “reverse blips” set to ‘on’, which requires an additional 25 minutes of acquisition time. NOTE: If the custom ‘reverse-blip’ sequence⁹ (required for susceptibility artifact correction during Step 3) is unavailable, only a single EPI phase encoding direction is possible, whereas the reversed blip sequence modification allows the choice of phase encoding direction (right-to-left or left-to-right).
7. When imaging is completed, remove the animal from the holder and return it to its cage. Do not leave an animal unattended until it has regained sufficient consciousness to maintain sternal recumbency.

3. Image Processing

1. Export data from the system in DICOM format directly from the system (preferable) or convert the data to NIFTI format using custom or third-party software.
2. Perform susceptibility artifact correction.
 1. Extract the b=0 volumes from each scan into a single file, using utilities provided with FSL or other MRI software packages. One file for each phase encode direction is required.
NOTE: For example, if each scan consisted of 8 scans of varying b-values with diffusion weighting in the transverse direction, followed by 8 scans of diffusion weighting in the longitudinal direction, the image file contains b=0 scans in the 1st and 9th volumes, and can be extracted and assembled with the following shell code:

```
fslroi ${up}_dwi_masked.nii.gz temp1 0 1
fslroi ${up}_dwi_masked.nii.gz temp2 8 1
fslroi ${down}_dwi_masked.nii.gz temp3 0 1
fslroi ${down}_dwi_masked.nii.gz temp4 8 1
fslmerge -t blip_both temp1 temp2 temp3 temp4
```

 (where in this case \$up and \$down are the scans with normal and reversed phase encode directions, respectively).
 2. Use the ‘topup’ command in fsl^{10,11} to create a corrected file with reduced image distortion artifacts. Apply this correction to the raw DWI images to be used for creation of parameter maps.
NOTE: Instructions for use of the command can be found at <http://fsl.fmrib.ox.ac.uk/fsl/fslwiki/TOPUP/TopupUsersGuide>. Example code to use the command in this case is as follows:

```
topup --imain=blip_both_nlmf_b0images_masked.nii --datain=../topup_data.txt --config=./b02b0_ratspine.cnf --out=topup_splines_nlmf
--iout=$out --verbose --logout=topuplog.log
dwiup='ls ${up}*dwi_nlmFilt.nii'
dwi down='ls ${down}*dwi_nlmFilt.nii'
applytopup --imain=${dwiup},${dwi down} --datain=../topup_data.txt --method=jac --inindex=1,$ind --topup=topup_splines_nlmf --
out=DWI_${out} --v
Copy and edit the default file in ${FSLDIR}/etc/flirtsch/b02b0.cnf for the rat spinal cord by reducing each of the values in the --warpres
and --fwhm lines by a factor of 10.
```
3. If images with diffusion weighting are acquired along at least 6 non orthogonal directions (using a DTI scheme in Paravision or a similar custom design), use software packages such as fsl’s Diffusion Toolbox¹² or Camino¹³ to calculate standard DTI parameter maps. If not, use a custom procedure for generating useful metrics, which employs diffusion weighting only along 2 directions, for example, as indicated in steps 3.4 onward.
4. Load the corrected DWI file outputted by TOPUP into fslview and select “File -> Create Mask” from the menu. Use the pencil tools to draw a region of interest within one tissue type (for example GM, dorsal WM, or ventrolateral WM). Save this file and repeat for any other desired ROIs to use later.
NOTE: Other procedures to segment ROIs from the spinal cord have been documented^{14,15} and may be preferable for advanced users.
5. Use the ROI file to mask the DWI file and then calculate the mean signal within the ROI for each image volume using the following command:

```
fsstats -t DWI_corrected.nii.gz -k GM_mask.nii.gz -M
```
6. Copy the first 8 results into numerical computing program such as MATLAB, as a vector for transverse signal (for example call it sig_T), and the second 8 results as a vector for longitudinal signal (sig_L), where 8 is the number of b-values used.
 1. Copy the b-values in a numerical computing program as a vector of 8 b-values. The b-values for the transverse and longitudinal directions were identical. If possible, the effective b-value, rather than the nominal b-value, should be obtained from the scanner, which is listed in the parameter window from step 2.3.5 as “Effective B value”.
 2. Use the numerical computing program’s curve fitting toolbox to fit the signal vs. b-value data to the desired model by typing cftools at the command prompt. To do this, click “Data...” and select the signal vectors as y-data and the b-values as x-data. Click “Fitting...” and under “Type of fit” choose “Custom Equation,” then click “New” and “General Equations” to enter an equation for fitting.
7. To fit to the standard diffusion model, enter the equation:
 $S_0 \cdot \exp(-x \cdot D)$ (1)
8. To fit to a model which includes diffusion and a second order term (kurtosis; K) to measure the deviation from gaussian diffusion¹⁶, enter the equation:
 $S_0 \cdot \exp(-x \cdot D + (1/6) \cdot (x \cdot D)^2 \cdot K)$ (2)
9. Click “OK” and “Apply”. Observe the estimated values for diffusivity (D) and kurtosis (K) on the output window. In the “Data Set:” selector, select the sig_T (or sig_L) data for use with equation (1) or (2) and click “Apply”.
10. Calculate the anisotropy index (AI) using the transverse and longitudinal diffusivities:
 $AI = (D_L - D_T) / (D_L + D_T)$ (3)

This is analogous to the fractional anisotropy (FA) calculated from the DTI model. An anisotropy index for kurtosis can also be calculated using transverse and longitudinal kurtosis in place of diffusivity.
 NOTE This method gives values of model parameters such as K_T , D_T , etc. It is also possible to use the command-line operation of the curve fitting toolbox on each voxel within the spine to create a map of each parameter from the model. Alternative fitting methods may be used and are detailed elsewhere.¹⁷

Representative Results

Proper procedures to minimize motion artifacts result in high-quality diffusion weighted images of the rat cervical spinal cord. Using custom respiratory gating (**Figure 2**), saturating unwanted signal from tissues outside the spine (**Figures 3B & C**), and magnetic field susceptibility distortion correction produces diffusion-weighted images such as those in **Figures 4 and 5**. Improper or un-gated images will lead to artifacts in the form of ghosting (**Figure 3E**), whereas correct gating is free of artifacts.

Visual inspection of the diffusion weighted images across the 12 slices reveals features of the spinal cord that relates to its microstructure. Specifically, faster diffusion in the tissue results in greater signal loss on diffusion weighted images, which is exacerbated with greater diffusion weighting (b-value). With diffusion weighting performed perpendicular to the spinal cord axis, white matter along the periphery of the cord appears bright, since the diffusion is slow and restricted perpendicular to the axons. In contrast, the gray matter within the central region of the cord appears darker, since it is composed of axons and cell bodies that are not all aligned along a single direction. In comparison, diffusion weighting in the parallel direction results in white matter with a darker appearance, since diffusion is fast along the axons, whereas gray matter is relatively brighter. It is important to note that the separate diffusion weighted images are shown for different b-values, since the parallel and perpendicular directions have the best contrast between white and gray matter at different b-values.

Combining all of the diffusion weighted images using mathematical formalisms allows maps of the diffusion parameters to be shown. The average signals from the white and gray matter are plotted against the diffusion weighting factor (b-value) for the parallel and perpendicular directions. This quantitative data reinforces the diffusion weighted images shown in **Figure 4**. Specifically, white matter has a strong dependence on the direction of the diffusion weighting (longitudinal or transverse), whereas gray matter is less dependent on the direction. Similarly, fitting of the signal at each voxel using the equation for diffusion kurtosis yields quantitative maps of diffusion parameters (**Figure 6B**), which highlight this same dependence. White matter has a high degree of anisotropy for both the diffusion (AID) and kurtosis measurements (AIK). Thus, transverse diffusion and kurtosis reveal the underlying microstructure of the spinal cord that is known from histological studies. These diffusion parameters, which are acquired in live, but anesthetized animals, reflect microscopic tissue properties such as axon density and diameter. Alterations in these measures caused by injury and disease will be useful for noninvasively evaluating the consequences of injury and the effects of promising therapies. Diffusion weighted imaging of the rat cervical spinal cord may therefore become a tool for preclinical studies of spinal cord injury and diseases of the spinal cord.

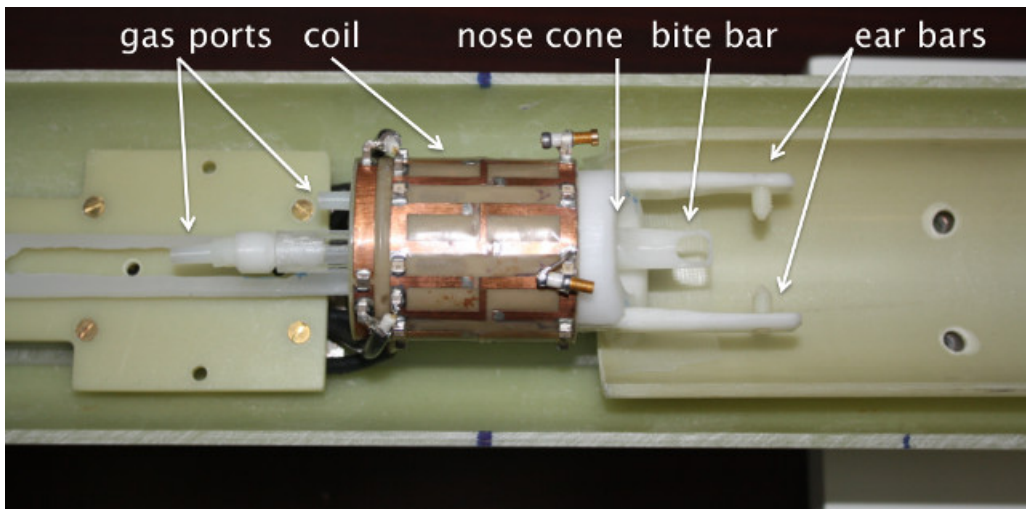


Figure 1: Design of the coil and holder for cervical spinal cord MRI. A custom quadrature volume coil (Doty Scientific Inc) was used to image the cervical spine with high sensitivity and uniformity. Anesthesia and medical air are delivered by the indicated gas ports into the nose cone, which fits comfortably around the nose of the rat. Exhaled and excess gas is captured by the exhaust line under slight vacuum. The head of the rat is secured with the bite bar placed around the incisors and the ear bars placed delicately within the ear canal. Other physiologic monitoring components, including the respiratory monitor and temperature probe are not shown.

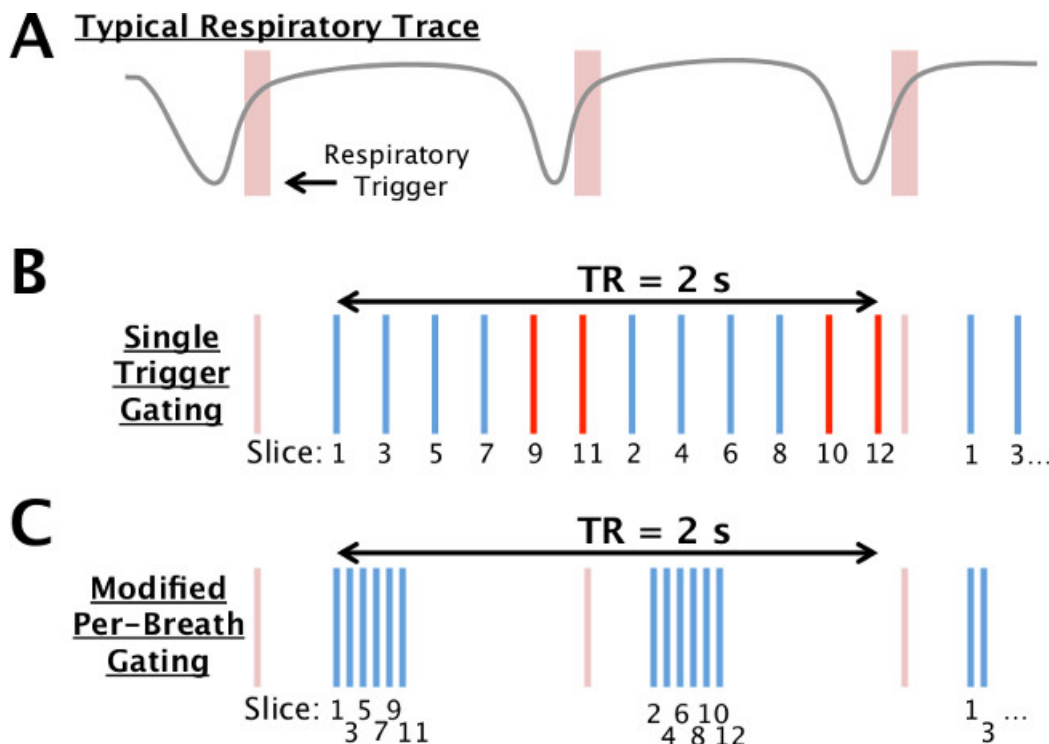


Figure 2: Respiratory gating scheme. A typical respiratory trace (gray) and trigger (red) from the gating unit are shown schematically (A). In the typical implementation of gating (B), a single trigger is used to acquire all slices (vertical lines; 12 shown here) at times evenly-spaced within the repetition time (TR). If the TR exceeds the typical period, several slices may occur during a breath and be susceptible to motion (red). In the modified scheme (C), a subset of slices are acquired rapidly after the trigger (6 shown here) followed by a delay, with the other slices acquired after the subsequent trigger. Effectively, the TR is identical between the two schemes by rearranging the delays within the sequence.

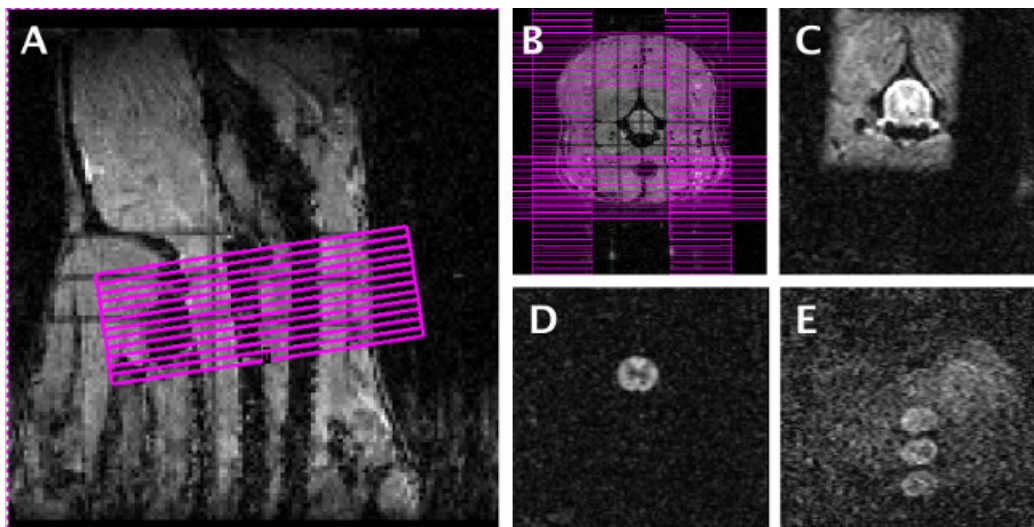


Figure 3: MRI slice positioning, saturation bands, and motion control. Twelve axial slices were arranged on the scout image (A) with the most anterior slice positioned at a consistent distance from the intersection of the brainstem and cerebellum. Saturation bands (B) were added to eliminate unwanted signal outside the area of interest. An image without diffusion weighting (C) and one with diffusion weighting (D) with the custom gating scheme employed clearly show the anatomy of the cord and is free of artifacts. With the non-optimized gating scheme or improper respiratory gating, diffusion weighted images show artifacts (E) as a loss of signal within the cord, or multiple “ghosts” outside the cord that will corrupt subsequent analysis. [Please click here to view a larger version of this figure.](#)

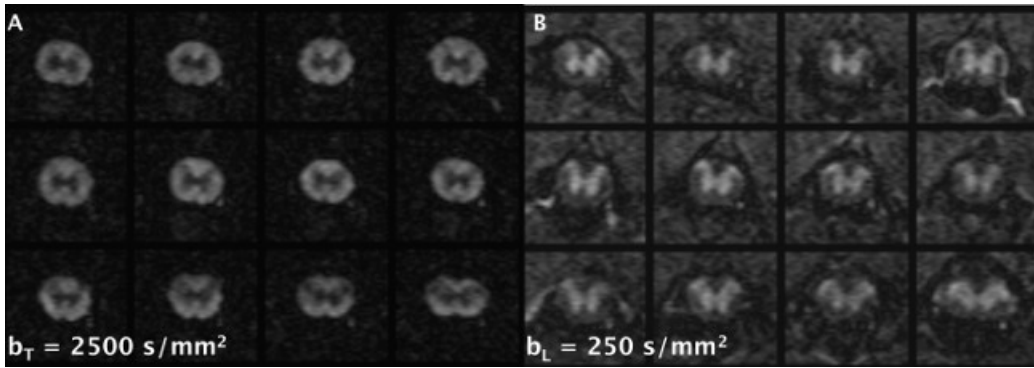


Figure 4: Representative diffusion weighted images. Using the optimizations described in the text, high-quality diffusion weighted images were obtained with diffusion weighting applied transverse (A) and longitudinal (B) to the spinal cord main axis. Different b-values are shown for each direction that provide the best contrast between the white and gray matter for illustrative purposes. For each direction or b-value, all 12 slices were acquired in approximately 90 sec. [Please click here to view a larger version of this figure.](#)

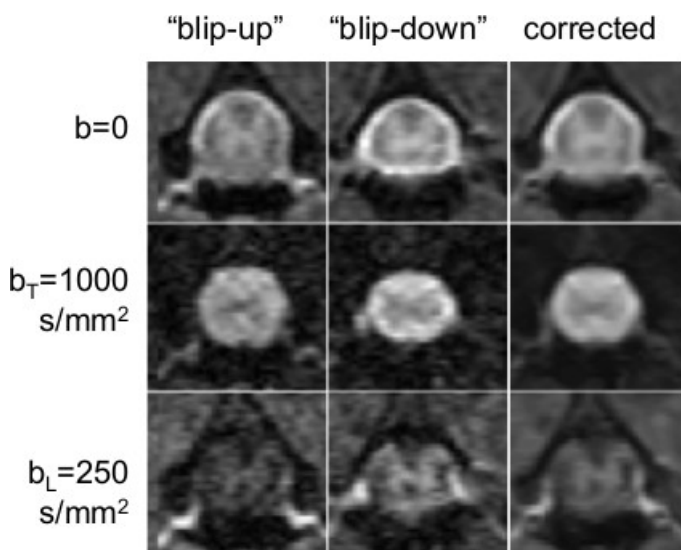


Figure 5: Reversed phase-encode correction process. The left column shows a single slice imaged with the DWI sequence as outlined in this protocol (“blip up” image). The middle column shows the sequence acquired a second time with the “reverse blips” set to ‘on.’ Note how features that appear stretched in the first image appear compressed in the middle column. The right column shows the diffusion weighted images corrected using TOPUP. The top row is the non-diffusion weighted image, the middle row is an example with diffusion weighting applied in the transverse direction, and the bottom row is an example with diffusion weighting applied in the longitudinal direction. [Please click here to view a larger version of this figure.](#)

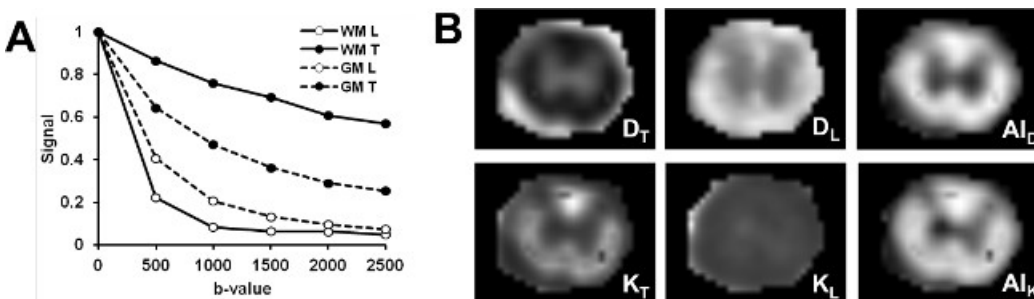


Figure 6: Computed maps of diffusivity and kurtosis. The normalized signal (image intensity) is plotted (A) as a function of diffusion weighting (b-value) for the transverse (T) and longitudinal (L) diffusion encoding direction. High-quality maps (B) of diffusivity (D), kurtosis (K), and anisotropy (AI) are calculated from the signal at each voxel and reveal unique features of the spinal cord tissue. Specifically, there is clear difference in parameters between the white and gray matter, as well as regional differences in the white matter regions. [Please click here to view a larger version of this figure.](#)

Discussion

The techniques outlined here can provide high-quality diffusion weighted images of the rat spinal cord in vivo. Image quality depends on many factors, but the spinal cord has several unique issues that are important.

Motion is an important problem that if not corrected, will result in unusable images. Thus, it requires careful monitoring during the MRI session. If image artifacts are observed on the initial scan that are consistent with motion, stop the acquisition and take steps to eliminate the artifacts, since these are difficult to remove in post-processing. Ensure that the respiratory computer receives a strong, regular signal from the respiratory monitoring unit. The respiration belt may need to be adjusted for the correct tension that provides a consistent signal but does not restrict the animal's breathing. Maintain the appropriate level of anesthesia at all times; 1.5–2.0% isoflurane has been used in our experience. Likewise, reduction in the overall movement of the animal and the spine is another important aspect to provide artifact-free images. Unlike the human spinal cord, which experiences significant motion caused by CSF pulsation related to the cardiac cycle, CSF pulsation in the rodent is predominantly associated with the respiratory cycle¹⁸. While it is difficult to fully eliminate all motion in the cord, it is particularly important to reduce the motion to the extent possible, which is often achieved through trial and error. Furthermore, rats with various neurological injuries or disorders may have abnormal respiratory rates or other physiological complications that may require adaptation of the procedures outlined herein.

The modifications to the pulse sequence for respiratory gating, along with image reconstruction procedures tailored for this purpose, minimize the effects of distortion caused by inhomogeneous magnetic fields that cannot be removed by adjustments performed on the MRI system.

Similarly, image quality depends on the duration of imaging time. In our example, limiting the number of diffusion weighting along only two directions enabled a reduction in total imaging time. A limitation of this approach is that it is no longer compatible with full tensor analysis (DTI), which is the norm for many other studies. Alternatively, using fewer averages and more diffusion directions or b-values may allow for better characterization while maintaining the same acquisition time. Previous studies have shown that the 2-direction approach provides information consistent with the 6-direction (DTI) approach¹⁹, but care must be taken to ensure the slices (and diffusion directions) are oriented precisely along and perpendicular to the cord. However, acquiring multiple b-values allows for better characterization and mathematical fitting of kurtosis and is recommended over the use of a single b-value. Moreover, the full sequence was repeated with a reversed phase encode direction which reduces the effects of magnetic field susceptibility artifacts, and improves overall image quality through averaging. Finally, the image resolution used in our protocol provides clear separation of the white and gray matter. Images with higher resolution are possible, although this often comes at the expense of longer scan times or the potential for more artifacts.

Improvements in radiofrequency coils, pulse sequences, and post-processing methods will all have the effect of improving imaging of the spinal cord in future adaptations of this method. For example, surface coils may be beneficial for improved image quality similar to that observed in mice.²⁰ These measures have a high likelihood of being useful as biomarkers for clinical diagnosis and management of spinal cord injuries.

Disclosures

Publication fees for this article were partially sponsored by Bruker Corporation.

Acknowledgements

We thank Kyle Stehlik, Natasha Wilkins, and Matt Runquist for experimental assistance. Funded through the Research and Education Initiative Fund, a component of the Advancing a Healthier Wisconsin endowment at the Medical College of Wisconsin, and the Craig H. Neilsen Foundation.

References

1. Jirjis, M. B., Kurpad, S. N., Schmit, B. D. Ex Vivo Diffusion Tensor Imaging of Spinal Cord Injury in Rats of Varying Degrees of Severity. *J Neurotrauma*. **30**, (18), 1577-1586 (2013).
2. Basser, P. J., Mattiello, J., LeBihan, D. Estimation of the Effective Self-Diffusion Tensor from the NMR Spin Echo. *J Magn Reson*. **103**, (3), 247-254 (1994).
3. Basser, P. J., Mattiello, J., LeBihan, D. MR diffusion tensor spectroscopy and imaging. *Biophys J*. **66**, (1), 259-267 (1994).
4. Song, S. -K., Sun, S. -W., Ju, W. -K., Lin, S. -J., Cross, A. H., Neufeld, A. H. Diffusion tensor imaging detects and differentiates axon and myelin degeneration in mouse optic nerve after retinal ischemia. *NeuroImage*. **20**, (3), 1714-1722 (2003).
5. Beckmann, N., Bruttel, K., Urban, L., Rudin, M. Signal changes in the spinal cord of the rat after injection of formalin into the hindpaw: characterization using functional magnetic resonance imaging. *Proc Natl Acad Sci U S A*. **94**, (10), 5034-5039 (1997).
6. Le Bihan, D., Poupon, C., Amadon, A., Lethimonnier, F. Artifacts and pitfalls in diffusion MRI. *J Magn Reson Imaging*. **24**, (3), 478-488 (2006).
7. Ford, J. C., Hackney, D. B., et al. MRI characterization of diffusion coefficients in a rat spinal cord injury model. *Magn Reson Med*. **31**, (5), 488-494 (1994).
8. Clark, C. A., Barker, G. J., Tofts, P. S. Magnetic resonance diffusion imaging of the human cervical spinal cord in vivo. *Magn Reson Med*. **41**, (6), 1269-1273 (1999).
9. Mohammadi, S., Nagy, Z., Hutton, C., Josephs, O., Weiskopf, N. Correction of vibration artifacts in DTI using phase-encoding reversal (COVIPER). *Magn Reson Med*. **68**, (3), 882-889 (2012).
10. Andersson, J. L. R., Skare, S., Ashburner, J. How to correct susceptibility distortions in spin-echo echo-planar images: application to diffusion tensor imaging. *NeuroImage*. **20**, (2), 870-888 (2003).
11. Smith, S. M., Jenkinson, M., et al. Advances in functional and structural MR image analysis and implementation as FSL. *NeuroImage*. **23**, S208-S219 (2004).

12. Behrens, T. E. J., Woolrich, M. W., *et al.* Characterization and propagation of uncertainty in diffusion-weighted MR imaging. *Magn Reson Med.* **50**, (5), 1077-1088 (2003).
13. Cook, P. A., Bai, Y., *et al.* Camino: Open-Source Diffusion-MRI Reconstruction and Processing. *14th Scientific Meeting of the International Society for Magnetic Resonance in Medicine.* 2759 (2006).
14. Kim, J. H., Tu, T. -W., Bayly, P. V., Song, S. -K. Impact Speed Does Not Determine Severity of Spinal Cord Injury in Mice with Fixed Impact Displacement. *J Neurotrauma.* **26**, (8), 1395-1404 (2009).
15. Tu, T. -W., Kim, J. H., Yin, F. Q., Jakeman, L. B., Song, S. -K. The impact of myelination on axon sparing and locomotor function recovery in spinal cord injury assessed using diffusion tensor imaging. *NMR Biomed.* **26**, (11), 1484-1495 (2013).
16. Jensen, J. H., Helpert, J. A., Ramani, A., Lu, H., Kaczynski, K. Diffusional kurtosis imaging: The quantification of non-gaussian water diffusion by means of magnetic resonance imaging. *Magn Reson Med.* **53**, (6), 1432-1440 (2005).
17. Veraart, J., Sijbers, J., Sunaert, S., Leemans, A., Jeurissen, B. Weighted linear least squares estimation of diffusion MRI parameters: Strengths, limitations, and pitfalls. *NeuroImage.* **81**, 335-346 (2013).
18. Budgell, B. S., Bolton, P. S. Cerebrospinal Fluid Pressure in the Anesthetized Rat. *J Manipulative Physiol Ther.* **30**, (5), 351-356 (2007).
19. Tu, T. -W., Kim, J. H., Wang, J., Song, S. -K. Full Tensor Diffusion Imaging Is Not Required To Assess the White-Matter Integrity in Mouse Contusion Spinal Cord Injury. *J Neurotrauma.* **27**, (1), 253-262 (2010).
20. Kim, J. H., Song, S. -K. Diffusion tensor imaging of the mouse brainstem and cervical spinal cord. *Nat Protoc.* **8**, (2), 409-417 (2013).